J Mater Sci (2007) 42:2181–2188
DOI 10.1007/s10853-006-1011-x

Effect of water on the fatigue behaviour of a pa66/glass fibers composite material

S. Barbouchi · V. Bellenger · A. Tcharkhtchi · Ph. Castaing · T. Jollivet

Received: 16 August 2004 / Accepted: 23 September 2005 / Published online: 18 February 2007

Abstract The aim of this study is to evaluate the effect of the humidity on the long term behaviour of glass fiber reinforced thermoplastic in fatigue. Two sets of samples were studied, one set contained 0.2 wt% of water, the second 3.5 wt%. The fatigue tests are performed at a 10 Hz frequency, at room temperature and two various relative humidity ratios, 50% RH and 96% RH. The S–N curve of dried samples (0.2%) is above the one of humid samples (3.5%), the endurance limit at 10^7 cycles for dried samples is equal to 40 MPa against 35 MPa for the second set. For a given strain, the fatigue life is higher for humid samples because the induced stress is much lower due to the plasticizing effect of water. Though the tests are carried out at room temperature (23 °C), the sample temperature at the surface reaches values higher than Tg and whatever the applied strain, the matrix is in a rubbery state when the fracture occurs. On the basis of S.E.M. examinations, the following scenario is proposed: crack initiation at the fiber end, crack propagation along the fiber sides going with debonding, then crack propagation in the rubbery matrix.

S. Barbouchi · V. Bellenger (✉) · A. Tcharkhtchi
LIM, ENSAM 151 Bd de l'Hôpital, 75013 Paris, France
e-mail: veronique.bellenger@paris.ensam.fr

Ph.Castaing · T. Jollivet
CETIM, IPC, 74 Route de la Jonelière, BP 82617,
44326 Nantes Cedex 3, France

Introduction

Glass fiber reinforced thermoplastics are more and more used for mechanical or structural applications due to the progress in the injection molding process, in the numerical simulation and in the improvement of the properties obtained. In many applications, the parts are loaded to dynamic stresses; though the initiation and the propagation of fatigue cracks are known to be the major cause of reinforced polymer failure, it remains very important to study their fatigue behaviour in aggressive environments. Polymeric matrices submitted to a cyclic strain in the viscoelastic or viscoplastic domain absorb a part of the mechanical energy and dissipate it in the form of heat that has been generated as a result of internal frictions. During a fatigue test, the temperature of the material can increase and stabilize to some extent [1] but sometimes, in the case for instance where a high strain is applied, the temperature increases until the sample fracture occurs. Then we call it a thermal fracture. When the sample fracture is governed by crack initiation and propagation, it is called a mechanical fracture. The glass transition temperature of the PA66 matrix is not far from the ambient temperature and a temperature increase possibly induces a change in the matrix physical state. So the fatigue behaviour of our material strongly depends on temperature variations.

The behaviour of short glass fiber composite is strongly influenced by the matrix structure [2]. Though the fracture is initiated by a debonding at the matrix–fiber interface in most cases, there is a great difference between the fracture propagation within different polymer materials. The fracture propagation is fast in polystyrene, but much less favoured in polyethylene or

polyamide. The fatigue strength of polymers is governed by the resistance of the polymer to crack propagation. In spite of the discontinuities introduced by the presence of short fibers, the crack propagation rate obeys a classical PARIS law $\frac{da}{dN} = A\,\Delta K^m$ where $\frac{da}{dN}$ is the crack propagation rate and ΔK the stress intensity factor. For a carbon/polyamide composite, this law was modified [3] $\frac{da}{dN} = b[K_{\max}\,(1-R)^c]^r$ where $K_{\max}$ is the maximum value of the stress intensity factor and R is the $\frac{\sigma_{\min}}{\sigma_{\max}}$ ratio. The strength to crack growth is influenced by the water concentration [4]: for a PA66 with a degree of crystallinity of 40%, the fatigue crack propagation first decreases with the water content, passes through a minimum value for 2.5% of water content and then increases again until 8.5% of water content. A study of the fatigue behaviour of glass fiber/polyamide composite [5] shows that the damage occurs first at the fiber tip where the stress concentrations are the highest. Then microcracks propagate at the interface along the fiber and the matrix supports higher and higher stresses due to fiber debonding: locally these stresses possibly exceed the yield stress and the matrix undergoes a plastic strain. The fiber/matrix cohesion and the matrix ductility are both involved in the fracture mechanism of the material and for glass fiber/polyamide composite, both properties depend on the water concentration. The aim of our work is to examine the effect of water on the fatigue behaviour for this kind of composite.

Experimental

The matrix is a thermoplastic Polyamide 66 reinforced by short glass fibers. The fiber ratio was determined by a 2 h pyrolysis at 800 °C. The fraction crystallinity x_c was measured by DSC experiments. The apparatus is a NETZSCH DSC 200; three samples were heated from 30 °C to 310 °C at a heating rate of 2 °C/min. The fraction crystallinity is calculated by the ratio $\frac{\Delta H_m}{\Delta H_m^c}$ where ΔH_m is the experimental value of the specific enthalpy of fusion and ΔH_m^c is the melting enthalpy of the 100% crystalline polymer. $\Delta H_m^c = 188\,\mathrm{J\,g^{-1}}$ [6]. A specimen section perpendicular to the injection direction was observed by optical microscopy with an Olympus BH2-UMA. Fatigue tests were performed on two sets of samples. The first set was exposed to a humid environment (45% RH) at 25 °C and the second at the same temperature but 93% RH. The equilibrium water concentrations were 0.2% and 3.5% by weight. The glass transition was measured by viscoelasticimetry on a NETZSCH DMA apparatus. The initial mechanical properties were determined at 23 °C or at 130 °C and 50% HR in bending mode with an INSTRON 5402. The strain rate is $0.55 \times 10^{-3}\ \mathrm{s^{-1}}$ and the bending length is 60 mm. Fatigue tests were carried out with an ''alternative bending device'' [7] with a ratio $R = -1$, in two different atmospheres, 23 °C and 45% RH or 93% RH. Figure 1a shows the scheme of this device in which one end of the sample is in contact with grip of input testing shaft, while the other end is maintained between two fixed rollers. The geometry of samples is shown on Fig. 1b. The applied strain varies between 0.012 and 0.022. The most constrained part of the sample was determined by a linear elastic calculation Fig. 2; it is located at a distance of 18 mm from the embedded part. The surface temperature in this area was measured during the test by an infrared camcorder. Fractographic studies were conducted on a HITACHI-3200 N scanning electron microscope at an accelerating potential of 15 kV. Samples are gold metallized before analysis.

Results

Initial characteristics

The weight % of fibers determined on 6 samples is equal to 30.2 ± 0.03%. The fraction crystallinity measured by DSC is equal to 29 ± 1%. The length of glass fibers is 340 ± 180 μm and the diameter is 14 ± 1 μm. The major part of fibers is oriented in a direction parallel to the injection direction Fig. 3. The glass transition temperature was measured at 10 Hz frequency, it is equal to 70 °C for samples containing 0.2% H_2O (''dry'' samples) and –11 °C for samples containing 3.5% H_2O (''wet samples''). This difference

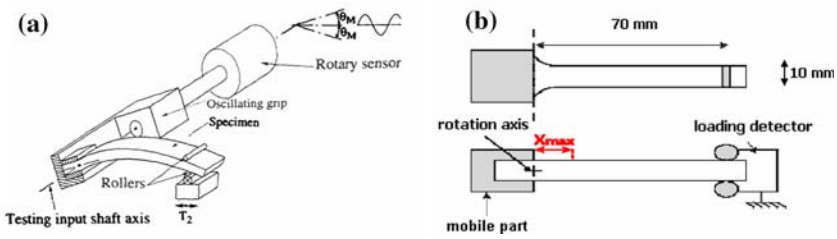

Fig. 1 Alternative bending device used for fatigue tests and specimen geometry

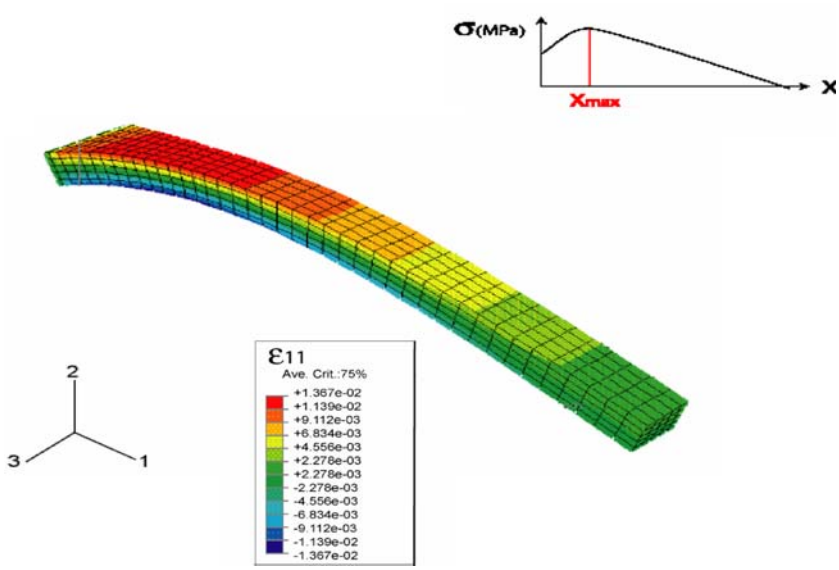

Fig. 2 Linear elastic calculation to determine the most constrained part of the sample

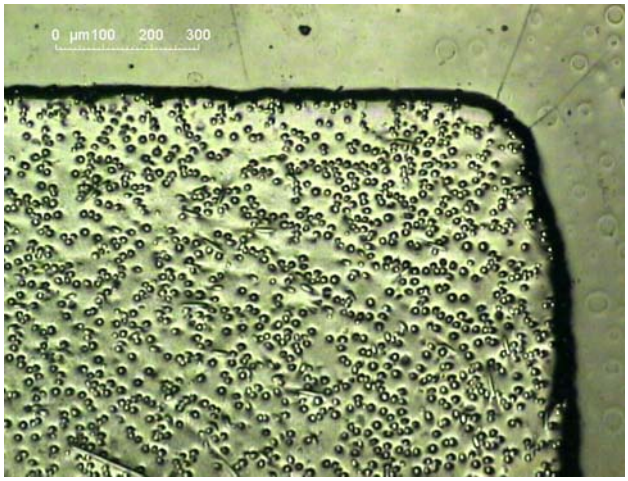

Fig. 3 Optical microscopy observation of the section perpendicular to the injection direction

is due to the plasticizing effect of water [8, 9], which suppresses some hydrogen bonding between amide groups, decreases the cohesive energy density and increases the mobility of polyamide chains. The effect of moisture content on Tg is similar for other polar polymers or for composites [10]: for each 1% water pick-up, Tg is lowered by about 20 °C. The mechanical properties are reported in Table 1. When the matrix is in a rubbery state (''dry'' sample at 130 °C and ''wet sample'' at 23 °C), the stress–strain curve displays a yield point. The elastic modulus and the ultimate stress decrease with the test temperature, whereas the ultimate elongation increases. The moisture effect on the mechanical properties of polyamide has been known for a long time [8, 9, 11]. Increasing water content involves a decreasing value of the Young's modulus and yield strength and increasing impact strength.

Table 1 Mechanicalcharacteristics measured in bending mode at 23 °C and130 °C

Water content in the specimen(wt%)	0.2	0.2	3.5
Testconditions	23 °C, 50% RH	130 °C, 50% RH	130 °C, 50%RH
E (MPa)	7550 ± 60	2790 ± 30	3700 ± 50
σ_R (MPa)	235 ± 2	93 ± 2	110 ± 5
ε_R(%)	3.7 ± 0.1	9.5 ± 0.3	9.0 ± 0.2
σ_y (MPa)	–	100 ± 1	124 ± 1
ε_y(%)	–	7.5 ± 0.1	7.4 ± 0.1

Fatigue tests

S–N curves

The S–N curves of dry (0.2% water) samples tested in 50% HR atmosphere and wet (3.5%) samples tested in 93% HR atmosphere do not display the same shape (Fig. 4). For the samples with 0.2% water content, the curve shows two different kinetic regimes.

1. There is a sharp decrease of stress maximum, $\sigma_{max,}$ during the first 1000 cycles.
2. The kinetic of fatigue behaviour then changes and maximum stress continues to decrease more slowly.
3. Even after 10^7 cycles, there is not a clear asymptotic value representative of an endurance limit, σ_{en}.

For the samples with 3.5% water content, only one kinetic regime was observed. In this case, the composite

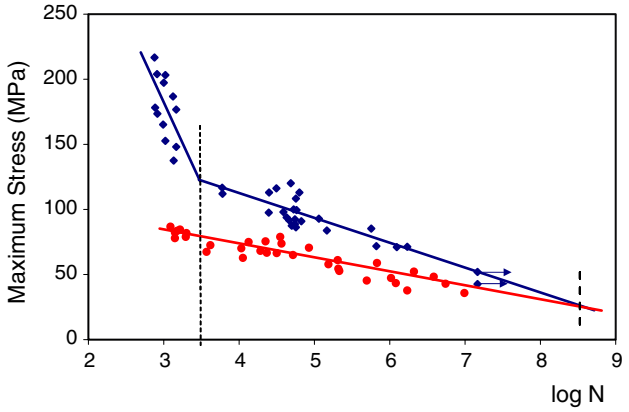

Fig. 4 S–N curve for the 30% glass-fibre-reinforced Polyamide 66, $R = -1$, $f = 10$ Hz, ◆, samples containing 0.2% H_2O tested at 23 °C and 50%HR, ● samples containing 3.5% H_2O tested at 23 °C and 90% HR

shows much lower resistance to the applied cyclic loading, but the maximum stress decreases with a lower rate.

It can be supposed when the break happens in the long term that the S–N curves intersect and in absence of asymptotic value, the wet sample shows higher fatigue strength.

For both kinds of samples (dried and wet) the points related to the different fatigue tests fall into a line which can be fitted according to Noda [12] by the following equation:

$$\sigma_{\max} = -A \log N + B \quad (1)$$

Where the slope A means the sensitivity of the fatigue resistance and the intercept B the apparent flexural strength. Table 2 shows the values of these constants for dried and wet samples. In the case of dry samples, the values of A and B are significantly higher for the first part than second part. In the first part of the S–N curve (from 10^0 to 10^3 cycles), the fatigue behaviour is governed by the effect of self heating, the sensitivity of fatigue resistance (A) is high and the apparent flexural strength (B) is much higher that the one measured in quasi-static bending tests (Table 1). A thermal fracture associated with high stresses and high strains is mainly observed. In the second part, there is a coupling effect of self heating and mechanical damage. The sensitivity of fatigue resistance (A) is smaller and the apparent flexural strength (B) is in the same order of magnitude than the one which we measured in static flexural tests at 130 °C (Table 1). For wet samples, a coupling effect of self heating, mechanical damage and moisture plasticization is observed. The sensitivity of fatigue resistance (A) is low and the apparent flexural strength (B) is equal to the value which we measured in quasi-static bending tests for the same samples at 130 °C (Table 1).

Table 2 The values of A and B determined by experimental fatigue tests

Constants	Dry samples (first part)	Dry samples (second part)	Wet samples (3.5% of absorbed water)
A (MPa)	610	20	10
B (MPa)	390	200	120

The σ/ε value of dry samples (Fig. 5a) and wet samples (Fig. 5b) is equal to the value of the Young modulus determined in quasi-static bending tests. For dry samples a sharp decrease of sample modulus is observed corresponding to the change of the matrix from the glassy state to the rubbery state. For wet samples, the matrix is in the rubbery state from the beginning of the test. The observed decrease in modulus, which is more progressive is possibly due to damage initiation. The plot of σ/ε versus the temperature for 0.2% H_2O samples (Fig. 6) is a kind of master-curve, which means that the modulus decreases in the same way when temperature increases whatever the cause.

Self heating

Figure 7 shows the temperature rise of dry and wet samples during fatigue tests. At least three different behaviours are shown: for high strain ($\varepsilon = 0.022$) and low water content (0.2%), the surface temperature of sample first increases slowly, then increases in an auto-accelerated way when the physical state of the matrix changes (the glass transition temperature Tg for dry samples is 70 °C). When the matrix is in a rubbery state, the temperature still increases until failure. For the same strain but high water content, the temperature increases more progressively: the plasticizing effect of water is equivalent to a decreasing strain. For a low water content and low strain ($\varepsilon = 0.014$), there is also an auto-accelerated increase of temperature at Tg but when the matrix is in a rubbery state, the temperature still increases but much more slowly. This auto-accelerated increase of temperature at Tg is due to the fast increase of the loss modulus E'' at Tg [13]. The dissipated heat Q per cycle and per volume unit at deformations with constant amplitude of strain is: $Q = \pi E'' \varepsilon_0^2$ where ε_0^2 is the maximum amplitude of strain during a cycle. For high water content (3.5%), the matrix is in a rubbery state from the test beginning, the temperature rises slowly and then reaches an equilibrium value, 130–150 °C before failure.

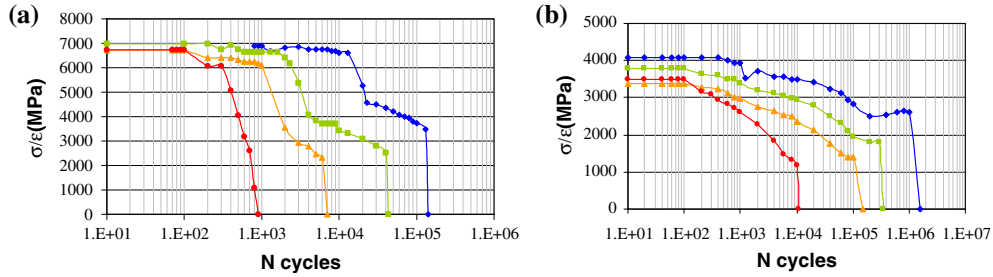

Fig. 5 Evolution of $\frac{\sigma}{\varepsilon}$ versus the number of cycles (**a**) for samples containing 0.2% H_2O, (**b**) for samples containing 3.5% H_2O, ♦ $\varepsilon = 0.012$, ■ $\varepsilon = 0.014$, ▲ $\varepsilon = 0.017$, ● $\varepsilon = 0.022$

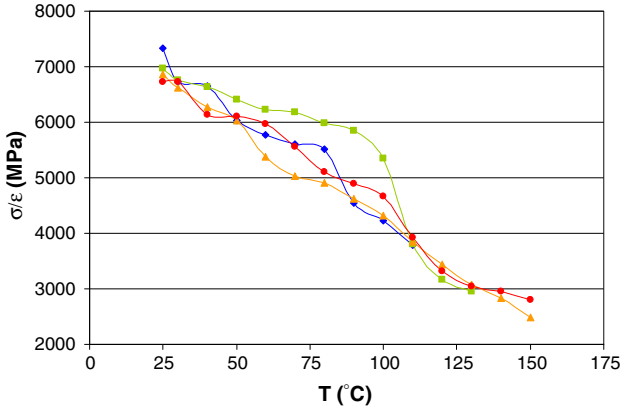

Fig. 6 Evolution of $\frac{\sigma}{\varepsilon}$ versus temperature for samples containing 0.2% H_2O, ♦ $\varepsilon = 0.012$, ■ $\varepsilon = 0.014$, ▲ $\varepsilon = 0.017$, ● $\varepsilon = 0.022$

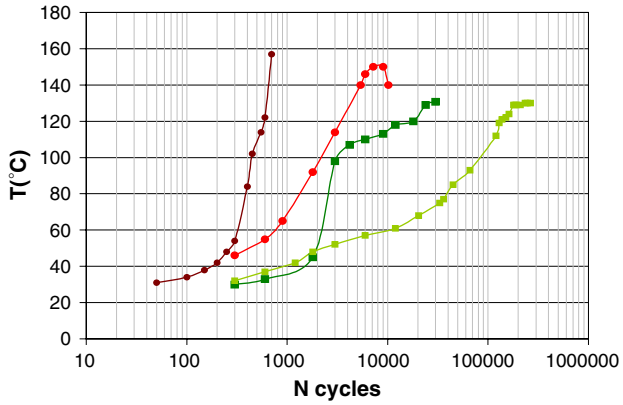

Fig. 7 Temperature increase versus the number of cycles, ● $\varepsilon = 0.014$ and 0.2% H_2O ■ $\varepsilon = 0.022$ and 0.2% H_2O, ● $\varepsilon = 0.014$ and 3.5% H_2O, ■ $\varepsilon = 0.022$ and 3.5% H_2O

Scanning electron microscopy of fracture surface

The examination of the fracture surface of specimens after quasi-static bending test at 23 °C (Fig. 8) shows that the fracture is ductile on sample edges and more brittle in the sample core, but generally speaking, it can be said that the fracture is brittle and ductile micro-domains are quite localized. For the sample tested at 130 °C, the failure surface is homogenous and characteristic of a ductile fracture (Fig. 9).

For short fatigue life time (high strain amplitude), the fracture surface displays flat featureless surfaces near the sample edges (Fig. 10a) whereas the central section of the sample thickness displays microductility (Fig. 10b) similar to the break surface, which we observed during the mechanical static tests at 130 °C. This microductility is indicative of extensive plastic deformation and drawing; it corresponds probably to the fast crack propagation during the last loading cycles assuming that the central section fails the latest. When the fracture surface is not flat and featureless close to sample edges, the classical fatigue break characteristics are noticed: microvoids, groups of curved arrest lines, damage propagation close to the fibers end, (Fig. 10c)... These characteristics also appear for samples with long fatigue life (Fig. 11). In the case of wet samples, there is no difference between the sample edges or central section and whatever the fatigue life, the fracture surfaces (Fig. 12) display the same microductility with a lot of debonding fibers. This important debonding could be due to the water attack on the matrix–fibers interface.

Discussion

Self heating

The phenomenon of self heating during cyclic loading of material composites was studied by several authors [14–16]. This self heating is related directly to the dissipated energy during fatigue tests. According to Chandra [17], it originates from:

The viscoelastic nature of matrix: In the case under study, the weight percentage of matrix is high (70%). One can say that each fibre particle is immersed in the matrix and surrounded by it; so the major contribution to composite damping is due to matrix. Even more, as

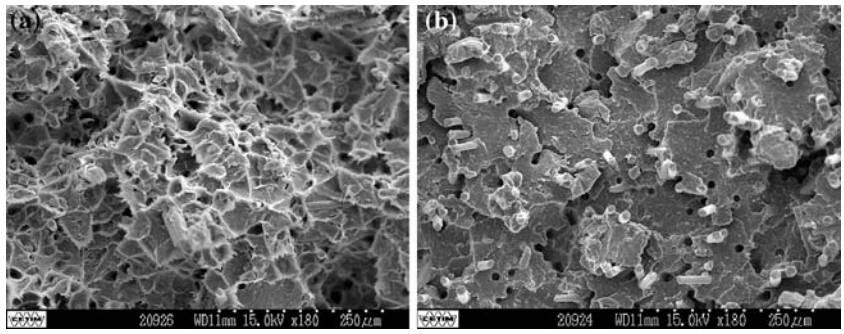

Fig. 8 S.E.M of failure surface for ''dry'' sample after static test at 23 °C, (**a**) sample edge, (**b**) sample core

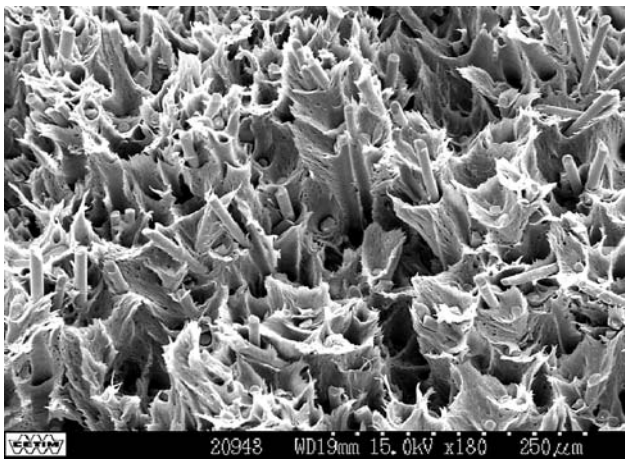

Fig. 9 S.E.M of failure surface for ''dry'' sample after static test at 130 °C

the glass transition temperature of dry (0.2% of water) PA66 is equal to 70 °C, this contribution is important.

The damping due to interphase polymer/fibre glass: The nature of interphase is different from the matrix and fibre ones, so its effect on damping is not the same. Composite damping is also related to the nature of this interphase. In the case under study the bonding between fibers and matrix is weak and could be a source (even low) of dissipated energy.

The damping induced by damage: After cracks initiation and during crack propagation, energy will be dissipated due to the damage in the region of matrix cracks.

The viscoplastic damping: Especially when the amplitude of applied strain is high, the main source of dissipated energy will be the non linear damping due

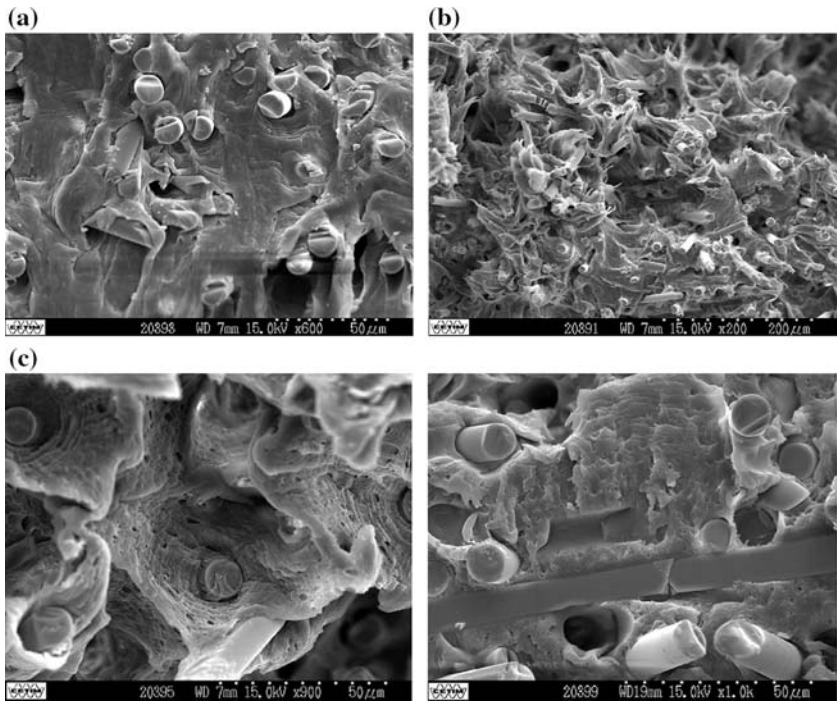

Fig. 10 S.E.M of fatigue failure surface for ''dry'' samples with short fatigue life (417 cycles) (**a**) specimen edge, (**b**) specimen core, (**c**) fatigue striations observed near sample edge

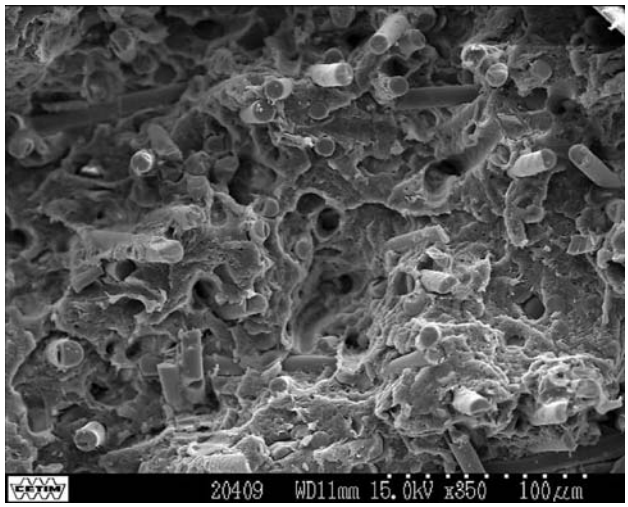

Fig. 11 S.E.M of fatigue failure surface for ''dry'' samples with long fatigue life (1.7×10^6 cycles); no difference is observed between the specimen core and edges

to the elasto-plastic behaviour of matrix. The temperature increases more rapidly (Fig. 5).

However, among these different sources of self-heating, the viscoelastic nature of matrix is the major one. In alternative (sinusoidal) fatigue test, stress and strain are not in phase, which induces the build-up of a hysteretic loop over a closed cycle. For a sinusoidal strain, the work W is equal to: $W = \omega\,\varepsilon_0^2\,(\int_0^{\frac{2\pi}{\omega}} E'\,\sin\omega t\,\cos\omega t\,\mathrm{d}t + \int_0^{\frac{2\pi}{\omega}} E''\,\cos^2\omega t\,\mathrm{d}t)$ where E' and E'' are respectively the storage modulus and loss modulus.

The first term of this equation is related to the elastic deformation and it is equal to zero. But the second term is due the energy dissipated during the test. After integration over one period $(2\pi/\omega)$ we will have: $W = \pi\varepsilon_0^2 E''$[13]. The mean mechanical dissipated power is $P_{\text{dissipated}} = -\frac{1}{2}\,\omega\,\varepsilon_0^2\,E''$. This mechanical energy will be converted to thermal energy. $Q = -P_{\text{dissipated}}$. The heat equation is $\frac{\mathrm{d}T}{\mathrm{d}t} = \frac{\lambda}{\rho\,c_p}\Delta T + \frac{Q}{\rho\,c_p}$, where λ = thermal conductivity (W/m.°C), ρ = density (kg m^{-3}) and C_p = specific heat (J kg^{-1} °C^{-1}). Using this equation, a relationship between the loss modulus (E'') and the temperature (T) can be established.

This self-heating phenomenon depending on applied stress and frequency was not taken into account in the study of Noda et al. [12] about the fatigue failure mechanisms of PA66/glass fibers. On the basis of various testing temperatures, they have shown that in the relationship $\sigma_{\max} = -A\,\log N + B$, A and B depend on temperature. This temperature dependence is different below and above the glass transition temperature indicating that the fatigue behaviour is governed at least by two different failure mechanisms. But the sample temperature and the testing temperature are not always the same. In our study all experiments used to plot the curves of Fig. 4, are performed at room temperature, but because of self heating phenomenon, the sample temperature corresponding to the different points does not remain the same. However it is possible to apply the model of Noda, which means that the constants A and B do not significantly depend on sample temperature.

Plasticizing effect of water

In Polyamide 66, water is tightly or loosely bound [9] depending on the water concentration. When the molar ratio water molecules/amide groups is less or equal to 1/3.6 [4], water is tightly bound by hydrogen bonding between two CO groups. Assuming that the water is only in the amorphous phase, this molar ratio corresponds in our samples to the weight % of 2.1%. For this ratio, a strong change in mechanical properties is observed; for instance the fatigue crack propagation rate passes through a minimum value. When the wt% of water exceeds 2.1%, water builds up aggregates of molecules loosely bound to amide groups. For the wet samples containing 3.5% water, there is a strong plasticizing effect of water as shown by the measurement of the elastic modulus (Table 1) of which value is divided by 2. Thus, the stress applied on the crack tip

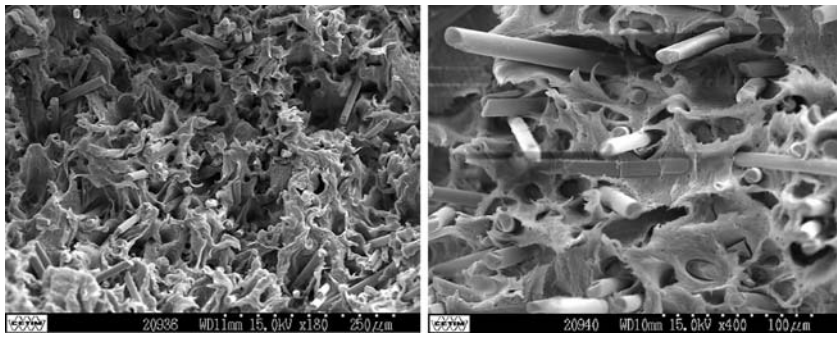

Fig. 12 S.E.M of ductile fatigue failure surface for samples containing 3.5% H_2O, $\varepsilon = 0.018$ with long fatigue life (3.5×10^4 cycles); no difference is observed between the specimen core and edges

by the bulk matrix ahead of it is lowered and the rate of the fatigue crack propagation increases. The damage induced per each loading cycle is higher for wet samples than for dry samples and for this reason, the endurance limit is smaller. This result agrees with the study of Bretz et al. [4] about the fatigue crack propagation (FCP) in PA66. The FCP was examined as a function of both stress intensity factor and water content. The FCP rate at a constant ΔK decreases when the water content increases up to 3% but then increases up to saturation. It should be noticed however that the difference between both endurance limits is low (40 MPa and 35 MPa) and that the fatigue behaviour is mainly governed by self-heating.

Fatigue failure scenario

The curves of dry samples stiffness ($\frac{\sigma}{\varepsilon}$) versus the number of cycles display four steps. During the first step the engineering stress is constant, localized cracks are initiated in the most constrained part of the sample e.g. the sample edge. According to SEM examinations (Figs. 10–12), it can be assumed that cracks initiate at fiber end and propagate at the interface along fibers. The second step is very short, the engineering stress decreases suddenly due to the change in the matrix physical state induced by self-heating. During the 3rd step, the matrix is in a rubbery state, the engineering stress still decreases in a monotonous way due to the increasing damage. At the end of this 3rd step, the fracture occurs suddenly: the defects concentration reaches a critical value, cracks propagate very fastly from the edge to the sample core with extensive plastic deformation and drawing of the matrix.

For wet samples, the first step of the curve $\frac{\sigma}{\varepsilon} = f$ (N cycles) is similar to the one of dry samples. It corresponds to crack initiation at the fiber ends in sample edges, which is possibly favoured by the water attack on the interface. The matrix is in a rubbery state at the beginning of the fatigue test, thus we do not observe the short second step. The 2nd step is analogous to the preceding 3rd step: the engineering stress decreases due to the increasing damage and fracture occurs suddenly when the microcracks concentration reaches a critical value. A localized increase of temperature at the crack tip in presence of a small amount of water favours localized plastic deformation and crack blunting, the crack propagation rate decreases. But in our case, all the matrix is in a rubbery state, the elastic modulus decrease involves an increase of the crack propagation rate since the crack tip is less constrained by the bulk matrix. This scenario is in god agreement with the S.E.M. observations made by Noda et al. [12]: damage initiation occurs at the fiber end near the sample edge where the stress concentration is the highest. Cracks propagate along the fiber sides by inducing fiber debonding and finally in the rubbery matrix involving a ductile fracture.

Conclusion

Water influences the fatigue behaviour of PA66/glass fiber composite material at room temperature and a 10 Hz frequency. The S–N curve of dried samples (0.2 wt% of water) tested with an alternative bending device is above the one of humid samples (3.5 wt%) and there is a low but significant difference in the values of endurance limit: it is equal at 10^7 cycles for dried samples to 40 MPa against 35 MPa for the ''humid'' samples. Though the tests are performed at room temperature, the 10 Hz frequency is enough high to induce a strong increase of the sample temperature. Whatever the applied strain, the matrix is in a rubbery state when the fracture occurs. On the basis of S.E.M. examinations, it can be set that cracks initiate at fiber ends, propagate along the fiber sides going with fiber debonding, then propagate in the rubbery matrix.

References

1. Trotignon JP, Tcharkhtchi A (1996) Macromol Symp 108:231
2. Dally JW, Carrillo DH (1969) Polym Eng Sci 9:434
3. Di Benedetto AT, Salee G (1975) Polym Eng Sci 15:243
4. Bretz PE, Hertzberg RW, Manson JA (1987) J Mater Sci 22:4015
5. Horst JJ, Damage 96 Conference, Fukuako, Japan, June 1996
6. Mark JE (1996) Physical properties of polymers handbook. American Chemical Society
7. Trotignon JP (1995) Polymer Testing 14:129
8. Mc Crum NG, Read BE, Williams G (1967) Anelastic and dielectric effects in polymeric solids. Wiley, New York
9. Papir YS, Kapur S, Rogers CE, Baer E (1972) J Polym Sci A2 10:1305
10. Wright WW (1981) Composites 12:201
11. Kohan MI (1973) Nylon plastics. Wiley, New York
12. Noda K, Takahara A, Kajiyama T (2001) Polymer 42:5803
13. Van Krevelen DW, Hoftyzer PJ (1976) Properties of polymers, 2nd edn. Elsevier, New York, p 283
14. Rittel D (2000) Mech Mater 32:131
15. Rittel D, Eliash N, Halary JL (2003) Polymer 44:2817
16. Molinari A, Germain Y (1996) Int J Solids 33(23):3439
17. Chandra R, Singh SP, Gupta K (1999) Compos Struct 46:41